Structural Engineering and Mechanics, Vol. 33, No. 5 (2009) 543-560
DOI: http://dx.doi.org/10.12989/sem.2009.33.5.543

Crack identification in short shafts using wavelet-based element and neural networks

Jiawei Xiang†

School of Mechantronic Engineering, Guilin University of Electronic Technology, Guilin, 541004, P.R. China
State Key Laboratory for Manufacturing Systems Engineering (Xi'an Jiaotong University)

Xuefeng Chen‡

State Key Laboratory for Manufacturing Systems Engineering (Xi'an Jiaotong University)

Lianfa Yang‡†

School of Mechantronic Engineering, Guilin University of Electronic Technology, Guilin, 541004, P.R. China

(Received September 27, 2007, Accepted September 24, 2009)

Abstract. The rotating Rayleigh-Timoshenko beam element based on B-spline wavelet on the interval (BSWI) is constructed to discrete short shaft and stiffness disc. The crack is represented by non-dimensional linear spring using linear fracture mechanics theory. The wavelet-based finite element model of rotor system is constructed to solve the first three natural frequencies functions of normalized crack location and depth. The normalized crack location, normalized crack depth and the first three natural frequencies are then employed as the training samples to achieve the neural networks for crack diagnosis. Measured natural frequencies are served as inputs of the trained neural networks and the normalized crack location and depth can be identified. The experimental results of fatigue crack in short shaft is also given.

Keywords: short shaft; wavelet-based element; neural networks; crack identification.

1. Introduction

The vibration-based crack identification methods include non-model-based and model-based methods have been rapidly expanding over the last few years (Dimarogonas 1996, Doebling 1998, Montalvão 2006).

The model-based method for damage and crack identification in structural components has acquired an important role in recent years. Some research involving the prediction of the response

† Associate Professor, Corresponding author, E-mail: wxw8627@163.com
‡ Professor, E-mail: Chenxf@mail.xjtu.edu.cn
‡† Professor, E-mail: y-lianfa@163.com

of structures to the presence of a transverse crack, and the detection of transverse cracks by the application of the linear facture mechanics theory. In order to evaluate the local flexibility or stiffness introduced by the crack, neglecting the effects that may be incorporated into the mass and damping matrices. In addition, it is assumed that the crack only affects the region adjacent to it. This additional flexibility or stiffness introduced by the crack can be calculated using the linear fracture mechanic theory (Papadopoulos and Dimarogonas 1987). Therefore, vibration behavior of cracked structures, in particular cracked shafts has received considerable attention in the last three decades (Sekhar and Srinivas 2002, Green and Casey 2005). There are two procedures, proposed in the technical literatures, to achieve the progress of crack detection in structures. The first procedure is forward problem analysis, which considers the construction of a crack stiffness matrix exclusively for the crack section, then the finite element model for crack structures is built up to gain modal parameters at various crack location and depth, such as natural frequencies, modal damping, modal mode etc. The second procedure is inverse problem analysis, which considers the measurement of dynamic parameters and numerical computing or searching for optimization values of crack location and depth according to the solving results of forward problem (Lee and Chung 2000, Lele and maiti 2002, Nandwana and Maiti 1997, Xiang and Chen 2006, 2007, Murigendrappa and Maiti 2005, Sinou 2007).

The most popular approach which is particularly well suited for modeling large-scale and complicated dynamic systems is the finite element method. Lele and Maiti (2002), investigated cracked short beam identification techniques based on the combination of forward and backward problems analysis. For the sake of crack singularity, eight-node iso-parametric elements are used to make more efficient calculation (Nandwana and Maiti 1997). However, both the numerical simulation and experimental studies cannot obtain satisfactory results. In order to gain accurate frequencies of structural systems, wavelet-based elements are employed as a high performance tool to fulfill the finite element analysis (Xiang and Chen 2006, 2007). The first three metrical frequencies are employed as inputs of the frequencies response functions. The intersection of the three frequencies contour lines (Owolabi and Swamidas 2003) predicted the normalized crack location and depth. However, in most experimental cases, the difference between measured frequencies and finite element solutions will make the above mentioned method failure. The difference caused by the numerical finite element modeling as compared to real structures. Then, the ‘zero-setting’ procedure that described by Adams (Adams and Cawley 1978) is used to improve the solution precision of inverse problem. In this procedure, Young’s modulus of the structure is changed by using the undamaged natural frequencies of the structure to determine an effective value. Obviously, ‘zero-setting’ procedure ascribes all the errors to Young’s modulus, which will distort the modal parameters of a real dynamic system.

Neural networks is a useful tool to deal with inverse problems in engineering. Liu proposed an inverse analysis method to simulate the A-scan ultrasonic nondestructive testing by means of back-propagation neural networks and computational mechanics (Liu 2002). Qu and Chen presented a two-step approach for diagnosing the joint damage of framed structures by using artificial neural networks (Qu and Chen 2003). Cho and Choi presented an efficient algorithm for the estimation of damage location and severity in bridge structures using probabilistic neural networks and applied to a cable-stayed bridge to verify its applicability (Cho and Choi 2004). Recognition of representative damages on returnable crates of beverages was carried out by an artificial neural networks trained exclusively with frequency response spectra from finite element simulations, which was proposed by Zachiarias (2004). Yuan developed a method focused on a neural networks method based on a

new damage signature for on-line damage detection applied to thin-walled composite structures (Yuan 2005). Lee and Yun thought that soft computing techniques such as neural networks and genetic algorithm had been utilized increasingly for the damage detection or assessment due to their excellent pattern recognition or optimization capability (Lee and Yun 2005). However, for the forward problem analysis, the traditional finite element method or computational methods are employed to build up crack detection database with bad precision. In addition, numerous dynamic response parameters will inevitably cause the huge input nodes of neural networks. Then the size of networks will increase accordingly and the corresponding usability and stability of the neural networks will be reduced enormously.

The desirable advantages of wavelet-based elements by using B-spline wavelet on the interval (BSWI) are multi-resolution properties and various basis functions for structural analysis (Canuto and Tabacco 1999, 2000). By means of "two-scale relations" of wavelets, the scale adopted can be changed freely according to requirements to improve analysis accuracy. Han, Ren and Huang successfully constructed some spline wavelet elements for analyzing structural mechanics problems under the theory frame of spline elements (Han *et al.* 2006). Xiang *et al.* construct C_0 and C_1 types transformation matrix to transfer the wavelet coefficients to physical degree of freedoms in finite element space, and classes of 1D and 2D BSWI elements for structural analysis with high performance (Xiang *et al.* 2006a, 2007a, 2007b, 2007c).

The purpose of the present work is to establish a method for predicting the normalized location and depth of transverse crack in short shaft by only considering the first three frequencies of the cracked shaft. We combine the wavelet-based finite element method with neural networks to make an effectively and accurately detection in cracked short shafts. Firstly, BSWI rotating Rayleigh-Timoshenko beam element is constructed to model and analysis short shaft and make a more effectively and accurately frequencies solutions. Then the surface fitting technique (Xiang and Chen 2006, 2007) is employed to achieve a precision crack detection database. The model-based inverse problems are solved by neural networks, which is a robust way to deal with inverse problem for crack detection in structures (Qu and Chen 2003, Cho and Choi 2004, Lee and Yun 2005).

2. A brief review of BSWI scaling functions

Classical approaches to wavelet construction deal with multiresolution analysis (MRA) on the

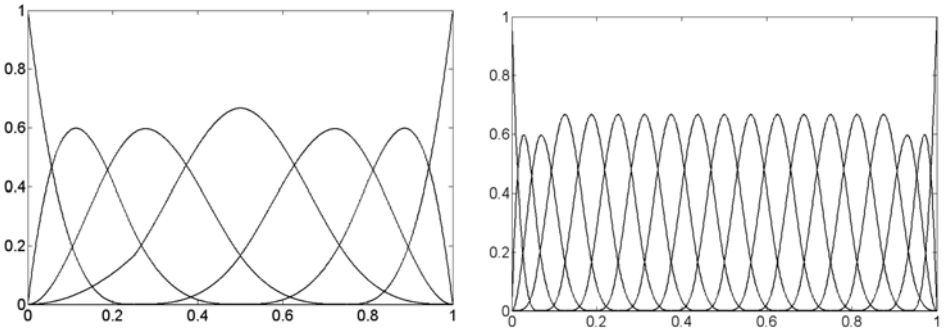

(a) $BSWI4_2$ (b) $BSWI4_4$

Fig. 1 BSWI scaling functions

entire real axis **R** or a function space $L^2(\mathbf{R})$. Sometimes the numerical oscillations will occur when the boundary value problems are solved by WFEM. To overcome this limitation, Chui, Quak and Goswami constructed BSWI functions, and presented a fast decomposition and reconstruction algorithm (Chui and Quak 1992, Goswami and Chui 1995). The scaling functions $\phi_{m,k}^{j}(\xi)$ for order m at the scale j are simply denote as BSWIm_j scaling functions. Some scaling functions are shown in Figs. 1(a), (b) respectively.

3. BSWI rotating Rayleigh-Timoshenko beam element

The static disc is modeled by a Rayleigh-Timoshenko beam considering the effects of the cross-section inertia and shear deformation, the elemental potential energy U^e can be written as (Nelson 1980)

$$U^e = \frac{1}{2}\int_0^{l_e}\left[EI_z\left(\frac{\mathrm{d}\theta_z}{\mathrm{d}x}\right)^2 + EI_y\left(\frac{\mathrm{d}\theta_y}{\mathrm{d}x}\right)^2\right]\mathrm{d}x + \frac{1}{2}\int_0^{l_e}\frac{GA}{k}\left[\left(\frac{\mathrm{d}w}{\mathrm{d}x}-\theta_z\right)^2 + \left(\frac{\mathrm{d}v}{\mathrm{d}x}-\theta_y\right)^2\right]\mathrm{d}x \tag{1}$$

where E is the Young's modulus, I_z and I_y is the moment of inertia, $w(\xi,t)$ and $v(\xi,t)$ are the transverse displacement, l_e is the elemental length, G is the shear modulus, A is the area of the cross-section, k is the shear deformation coefficient (In the present work, we suppose $k = 10/9$), and $\theta_z(x,t)$ and $\theta_y(x,t)$ are the rotation of the beam section due to bending.

The elemental kinetic energy T^e of the Rayleigh-Timoshenko beam allowing for the rotatory inertia effect and gyroscopic effect can be expressed as (Nelson 1980)

$$\begin{aligned} T^e = {} & \frac{1}{2}\int_0^{l_e}\rho A\left[\left(\frac{\partial w}{\partial t}\right)^2 + \left(\frac{\partial v}{\partial t}\right)^2\right]\mathrm{d}x + \frac{1}{2}\int_0^{l_e}\rho I_Z\left(\frac{\partial \theta_Z}{\partial t}\right)^2\mathrm{d}x + \frac{1}{2}\int_0^{l_e}\rho I_y\left(\frac{\partial \theta_y}{\partial t}\right)^2\mathrm{d}x \\ & -\Omega\int_0^{l_e}J_x\frac{\partial \theta_y}{\partial t}\theta_z\mathrm{d}x + \frac{\Omega^2}{2}\int_0^{l_e}J_x\mathrm{d}x \end{aligned} \tag{2}$$

where ρ is the density, A is the area of the cross-section, Ω is the rotational speed(rad/s), J_x is the polar moment of inertia.

Fig. 2 shows the nodal layout of BSWI rotating Rayleigh-Timoshenko beam element and the corresponding DOFs. We divide the standard solving domain Ω_e into $n = 2^j + m - 2$ segments, the node number = $n + 1$, Each node has four DOFs, i.e., $w_i, v_i, \theta_{z_i}, \theta_{y_i}$, $(i = 1, \ldots, n+1)$. The elemental whole DOF = $4(n + 1)$.

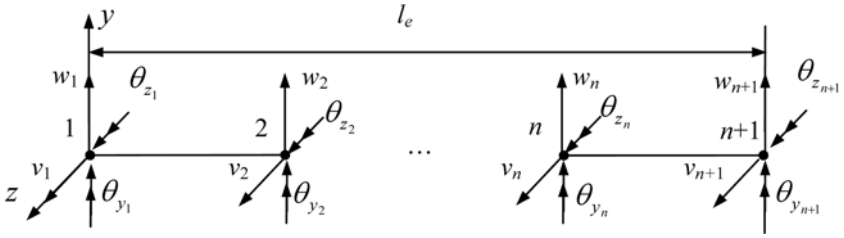

Fig. 2 The layout of elemental nodes and the corresponding DOF for BSWI rotating Rayleigh-Timoshenko beam element

The elemental physical DOFs can be represented by

$$\mathbf{u}^e = \{w_i \; v_1 \; \theta_{z_1} \; \theta_{y_1} \; w_2 \; v_2 \; \theta_{z_2} \; \theta_{y_2} \; \dots \; w_{n+1} \; v_{n+1} \; \theta_{z_{n+1}} \; \dots \; \theta_{y_{n+1}}\}^T \tag{3}$$

$w(\xi,t), v(\xi,t), \theta_z(\xi,t)$ and $\theta_y(\xi,t)$ can be independently interpolated by the BSWIm_j scaling functions as

$$\begin{cases} w(\xi,t) = \mathbf{\Phi}\mathbf{T}^e\mathbf{w}^e \\ v(\xi,t) = \mathbf{\Phi}\mathbf{T}^e\mathbf{v}^e \\ \theta_z(\xi,t) = \mathbf{\Phi}\mathbf{T}^e\boldsymbol{\theta}_z^e \\ \theta_y(\xi,t) = \mathbf{\Phi}\mathbf{T}^e\boldsymbol{\theta}_y^e \end{cases} \tag{4}$$

where

$$\begin{cases} \mathbf{w}^e = (w_1 \;\; w_2 \;\; \dots \;\; w_{n+1})^T \\ \mathbf{v}^e = (v_1 \;\; v_2 \;\; \dots \;\; v_{n+1})^T \\ \boldsymbol{\theta}_z^e = (\theta_{z_1} \;\; \theta_{z_2} \;\; \dots \;\; \theta_{z_{n+1}})^T \\ \boldsymbol{\theta}_y^e = (\theta_{y_1} \;\; \theta_{y_2} \;\; \dots \;\; \theta_{y_{n+1}})^T \end{cases} \tag{5}$$

C_0 type transformation matrix $\mathbf{T}^e$ is given by (Xiang *et al.* 2007b)

$$\mathbf{T}^e = ([\mathbf{\Phi}^T(\xi_1) \;\; \mathbf{\Phi}^T(\xi_2) \;\dots\; \mathbf{\Phi}^T(\xi_{n+1})^T])^{-1} \tag{6}$$

Substituting Eq. (4) into Eq. (1) and Eq. (2) respectively, we obtain

$$\begin{cases} U^e = \dfrac{1}{2}(\mathbf{w}^e)^{\mathrm{T}}\mathbf{K}_y^{e,1}(\mathbf{w}^e) + \dfrac{1}{2}(\mathbf{w}^e)^{\mathrm{T}}\mathbf{K}_y^{e,2}(\boldsymbol{\theta}_z^e) + \dfrac{1}{2}(\boldsymbol{\theta}_z^e)^{\mathrm{T}}\mathbf{K}_y^{e,3}(\mathbf{w}^e) + \dfrac{1}{2}(\boldsymbol{\theta}_z^e)^{\mathrm{T}}\mathbf{K}_y^{e,4}(\boldsymbol{\theta}_z^e) \\ \qquad \dfrac{1}{2}(\mathbf{v}^e)^{\mathrm{T}}\mathbf{K}_z^{e,1}(\mathbf{v}^e) + \dfrac{1}{2}(\mathbf{v}^e)^{\mathrm{T}}\mathbf{K}_z^{e,2}(\boldsymbol{\theta}_y^e) + \dfrac{1}{2}(\boldsymbol{\theta}_y^e)^{\mathrm{T}}\mathbf{K}_z^{e,3}(\mathbf{v}^e) + \dfrac{1}{2}(\boldsymbol{\theta}_y^e)^{\mathrm{T}}\mathbf{K}_z^{e,4}(\boldsymbol{\theta}_y^e) \\ T^e = \dfrac{1}{2}(\dfrac{\partial\mathbf{w}^e}{\partial t})^{\mathrm{T}}\mathbf{M}_y^{e,b}(\dfrac{\partial\mathbf{w}^e}{\partial t}) + \dfrac{1}{2}(\dfrac{\partial\mathbf{v}^e}{\partial t})^{\mathrm{T}}\mathbf{M}_z^{e,b}(\dfrac{\partial\mathbf{v}^e}{\partial t}) + \dfrac{1}{2}(\dfrac{\partial\boldsymbol{\theta}_z^e}{\partial t})^{\mathrm{T}}\mathbf{M}_y^{e,r}(\dfrac{\partial\boldsymbol{\theta}_z^e}{\partial t}) \\ \qquad + \dfrac{1}{2}(\dfrac{\partial\boldsymbol{\theta}_y^e}{\partial t})^{\mathrm{T}}\mathbf{M}_z^{e,r}(\dfrac{\partial\boldsymbol{\theta}_y^e}{\partial t}) - (\dfrac{\partial\boldsymbol{\theta}_y^e}{\partial t})^{\mathrm{T}}\mathbf{G}^e(\boldsymbol{\theta}_z^e) \end{cases} \tag{7}$$

where the elemental stiffness matrices can by solved by

$$\mathbf{K}_y^{e,1} = \mathbf{K}_z^{e,1} = \frac{GA}{kl_e}(\mathbf{T}^e)^{\mathrm{T}}\mathbf{\Gamma}^{1,1}(\mathbf{T}^e) \tag{8}$$

$$\mathbf{K}_y^{e,2} = \mathbf{K}_z^{e,2} = -\frac{GA}{k}(\mathbf{T}^e)^{\mathrm{T}}\mathbf{\Gamma}^{1,0}(\mathbf{T}^e) \tag{9}$$

$$\mathbf{K}_z^{e,3} = \mathbf{K}_y^{e,3} = (\mathbf{K}_y^{e,2})^{\mathrm{T}} \tag{10}$$

$$\mathbf{K}_y^{e,4} = \frac{EI_z}{l_e}(\mathbf{T}^e)^{\mathrm{T}}\mathbf{\Gamma}^{1,1}(\mathbf{T}^e) + \frac{GAl_e}{k}(\mathbf{T}^e)^{\mathrm{T}}\mathbf{\Gamma}^{0,0}(\mathbf{T}^e) \tag{11}$$

$$\mathbf{K}_z^{e,4} = \frac{EI_y}{l_e}(\mathbf{T}^e)^{\mathrm{T}}\boldsymbol{\Gamma}^{1,1}(\mathbf{T}^e) + \frac{GAl_e}{k}(\mathbf{T}^e)^{\mathrm{T}}\boldsymbol{\Gamma}^{0,0}(\mathbf{T}^e) \tag{12}$$

the translational mass matrices are

$$\mathbf{M}_y^{e,b} = \mathbf{M}_z^{e,b} = \rho A l_e (\mathbf{T}^e)^{\mathrm{T}}\boldsymbol{\Gamma}^{0,0}\mathbf{T}^e \tag{13}$$

the rotatory inertia mass matrices are

$$\mathbf{M}_y^{e,r} = \rho I_z l_e (\mathbf{T}^e)^{\mathrm{T}}\boldsymbol{\Gamma}^{0,0}(\mathbf{T}^e) \tag{14}$$

$$\mathbf{M}_z^{e,r} = \rho I_y l_e (\mathbf{T}^e)^{\mathrm{T}}\boldsymbol{\Gamma}^{0,0}(\mathbf{T}^e) \tag{15}$$

and the element gyroscopic matrix $\mathbf{G}^e$ is

$$\mathbf{G}^e = \Omega J_x l_e (\mathbf{T}^e)^{\mathrm{T}}\boldsymbol{\Gamma}^{0,0}\mathbf{T}^e \tag{16}$$

in which

$$\begin{cases} \boldsymbol{\Gamma}^{1,0} = \int_0^1 \dfrac{\mathrm{d}\boldsymbol{\Phi}^{\mathrm{T}}}{\mathrm{d}\xi}\boldsymbol{\Phi}\mathrm{d}\xi \\ \boldsymbol{\Gamma}^{1,1} = \int_0^1 \dfrac{\mathrm{d}\boldsymbol{\Phi}^{\mathrm{T}}}{\mathrm{d}\xi}\dfrac{\mathrm{d}\boldsymbol{\Phi}}{\mathrm{d}\xi}\mathrm{d}\xi \\ \boldsymbol{\Gamma}^{0,0} = \int_0^1 \boldsymbol{\Phi}^{\mathrm{T}}\boldsymbol{\Phi}\mathrm{d}\xi \end{cases} \tag{17}$$

Applying Hamilton's principle to the elemental Lagrangian function L, we can obtain the elemental free vibration equation

$$\mathbf{M}^e\begin{bmatrix} \dfrac{\partial^2\mathbf{w}^e}{\partial t^2} \\ \dfrac{\partial^2\mathbf{v}^e}{\partial t^2} \\ \dfrac{\partial^2\boldsymbol{\theta}_z^e}{\partial t^2} \\ \dfrac{\partial^2\boldsymbol{\theta}_y^e}{\partial t^2} \end{bmatrix} + \mathbf{g}^e\begin{bmatrix} \dfrac{\partial\mathbf{w}^e}{\partial t} \\ \dfrac{\partial\mathbf{v}^e}{\partial t} \\ \dfrac{\partial\boldsymbol{\theta}_z^e}{\partial t} \\ \dfrac{\partial\boldsymbol{\theta}_y^e}{\partial t} \end{bmatrix} + \mathbf{K}^e\begin{bmatrix} \mathbf{w}^e \\ \mathbf{v}^e \\ \boldsymbol{\theta}_z^e \\ \boldsymbol{\theta}_y^e \end{bmatrix} = 0 \tag{18}$$

where $\mathbf{M}^e$, $\mathbf{g}^e$ and $\mathbf{K}^e$ are the element mass, gyroscope and stiffness matrices respectively, which are given by

$$\mathbf{M}^e = \begin{bmatrix} \mathbf{M}_y^{e,b} & & & \\ & \mathbf{M}_z^{e,b} & & \\ & & \mathbf{M}_y^{e,r} & \\ & & & \mathbf{M}_z^{e,r} \end{bmatrix} \tag{19}$$

$$\mathbf{g}^e = \begin{bmatrix} 0 & 0 & 0 & 0 \\ 0 & 0 & 0 & 0 \\ 0 & 0 & 0 & \mathbf{G}^e \\ 0 & 0 & -\mathbf{G}^e & 0 \end{bmatrix} \tag{20}$$

$$\mathbf{K}^e = \begin{bmatrix} \mathbf{K}_y^{e,1} & 0 & \mathbf{K}_y^{e,2} & 0 \\ 0 & \mathbf{K}_z^{e,1} & 0 & \mathbf{K}_z^{e,2} \\ \mathbf{K}_y^{e,3} & 0 & \mathbf{K}_y^{e,4} & 0 \\ 0 & \mathbf{K}_z^{e,3} & 0 & \mathbf{K}_z^{e,4} \end{bmatrix} \tag{21}$$

According to the layout of elemental physical DOFs Eq. (3), Eq. (18) can be rewritten as

$$\overline{\mathbf{M}}^e \frac{\partial^2 \mathbf{u}^e}{\partial t^2} + \overline{\mathbf{G}}^e \frac{\partial \mathbf{u}^e}{\partial t} + \overline{\mathbf{K}}^e \mathbf{u}^e = 0 \tag{22}$$

Where the element mass matrix is

$$\overline{\mathbf{M}}^e = \begin{bmatrix} \overline{\mathbf{M}}_{1,1}^e & \overline{\mathbf{M}}_{1,2}^e & \cdots & \overline{\mathbf{M}}_{1,n+1}^e \\ \overline{\mathbf{M}}_{2,1}^e & \overline{\mathbf{M}}_{2,2}^e & \cdots & \overline{\mathbf{M}}_{2,n+1}^e \\ \cdots & \cdots & \cdots & \cdots \\ \overline{\mathbf{M}}_{n,1}^e & \overline{\mathbf{M}}_{n,2}^e & \cdots & \overline{\mathbf{M}}_{n,n+1}^e \\ \overline{\mathbf{M}}_{n+1,1}^e & \overline{\mathbf{M}}_{n+1,2}^e & \cdots & \overline{\mathbf{M}}_{n+1,n+1}^e \end{bmatrix} \tag{23}$$

in which

$$\overline{\mathbf{M}}_{p,q}^e = \begin{bmatrix} m_{y,p,q}^{e,b} & & & \\ & m_{z,p,q}^{e,b} & & \\ & & m_{y,p,q}^{e,r} & \\ & & & m_{z,p,q}^{e,r} \end{bmatrix} (p,q = 1,2,\cdots,n+1) \tag{24}$$

in which $m_{y,p,q}^{e,b}, m_{z,p,q}^{e,b}, m_{y,p,q}^{e,r}$ and $m_{z,p,q}^{e,r}$ are the corresponding entries of mass matrices $\mathbf{M}_y^{e,b}$, $\mathbf{M}_z^{e,b}, \mathbf{M}_y^{e,r}$ and $\mathbf{M}_z^{e,r}$.

the element gyroscope matrix is

$$\overline{\mathbf{G}}^e = \begin{bmatrix} \overline{\mathbf{G}}_{1,1}^e & \overline{\mathbf{G}}_{1,2}^e & \cdots & \overline{\mathbf{G}}_{1,n+1}^e \\ \overline{\mathbf{G}}_{2,1}^e & \overline{\mathbf{G}}_{2,2}^e & \cdots & \overline{\mathbf{G}}_{2,n+1}^e \\ \cdots & \cdots & \cdots & \cdots \\ \overline{\mathbf{G}}_{n,1}^e & \overline{\mathbf{G}}_{n,2}^e & \cdots & \overline{\mathbf{G}}_{n,n+1}^e \\ \overline{\mathbf{G}}_{n+1,1}^e & \overline{\mathbf{G}}_{n+1,2}^e & \cdots & \overline{\mathbf{G}}_{n+1,n+1}^e \end{bmatrix} \tag{25}$$

in which

$$\overline{\mathbf{G}}_{p,q}^e = \begin{bmatrix} 0 & 0 & 0 & 0 \\ 0 & 0 & 0 & 0 \\ 0 & 0 & 0 & g_{p,q}^e \\ 0 & 0 & -g_{p,q}^e & 0 \end{bmatrix} (p,q = 1,2,\cdots,n+1) \tag{26}$$

$g^e_{p,q}$ is the corresponding entries of gyroscope matrix $\mathbf{G}^e$.
and the element stiffness matrix is

$$\overline{\mathbf{K}}^e = \begin{bmatrix} \overline{\mathbf{K}}^e_{1,1} & \overline{\mathbf{K}}^e_{1,2} & \cdots & \overline{\mathbf{K}}^e_{1,n+1} \\ \overline{\mathbf{K}}^e_{2,1} & \overline{\mathbf{K}}^e_{2,2} & \cdots & \overline{\mathbf{K}}^e_{2,n+1} \\ \cdots & \cdots & \cdots & \cdots \\ \overline{\mathbf{K}}^e_{n,1} & \overline{\mathbf{K}}^e_{n,2} & \cdots & \overline{\mathbf{K}}^e_{n,n+1} \\ \overline{\mathbf{K}}^e_{n+1,1} & \overline{\mathbf{K}}^e_{n+1,2} & \cdots & \overline{\mathbf{K}}^e_{n+1,n+1} \end{bmatrix} \tag{27}$$

in which

$$\overline{\mathbf{K}}^e_{p,q} = \begin{bmatrix} k^{e,1}_{y,p,q} & 0 & k^{e,2}_{y,p,q} & 0 \\ 0 & k^{e,1}_{z,p,q} & 0 & k^{e,2}_{z,p,q} \\ k^{e,3}_{y,p,q} & 0 & k^{e,4}_{y,p,q} & 0 \\ 0 & k^{e,3}_{z,p,q} & 0 & k^{e,4}_{z,p,q} \end{bmatrix} (p,q = 1,2,\cdots,n+1) \tag{28}$$

in which $k^{e,1}_{y,p,q}$ $k^{e,2}_{y,p,q}$, $k^{e,3}_{y,p,q}$, $k^{e,4}_{y,p,q}$, $k^{e,1}_{z,p,q}$, $k^{e,2}_{z,p,q}$, $k^{e,3}_{z,p,q}$, $k^{e,4}_{z,p,q}$ are the entries of stiffness matrices $\mathbf{K}^{e,1}_y$, $\mathbf{K}^{e,2}_y$, $\mathbf{K}^{e,3}_y$, $\mathbf{K}^{e,4}_y$, $\mathbf{K}^{e,1}_z$, $\mathbf{K}^{e,2}_z$, $\mathbf{K}^{e,3}_z$, $\mathbf{K}^{e,4}_z$.

Assemble elemental free vibration equation to global solving equation, we have

$$\overline{\mathbf{M}}\frac{\partial^2 \mathbf{u}}{\partial t^2} + \overline{\mathbf{G}}\frac{\partial \mathbf{u}}{\partial t} + \overline{\mathbf{K}}\mathbf{u} = 0 \tag{29}$$

For the sake of computational purposes, Eq. (27) is written in the first order state vector form as

$$\mathbf{E}\frac{\partial \mathbf{q}}{\partial t} + \mathbf{F}\mathbf{q} = 0 \tag{30}$$

in which

$$\mathbf{q} = \begin{bmatrix} \frac{\partial \mathbf{u}}{\partial t} \\ \mathbf{u} \end{bmatrix} \tag{31}$$

$$\mathbf{E} = \begin{bmatrix} 0 & -\overline{\mathbf{M}} \\ \overline{\mathbf{M}} & \overline{\mathbf{G}} \end{bmatrix} \tag{32}$$

$$\mathbf{F} = \begin{bmatrix} \overline{\mathbf{M}} & 0 \\ 0 & \overline{\mathbf{K}} \end{bmatrix} \tag{33}$$

The associated eigenvalue problem for Eq. (30) is sought from an assumed solution form as

$$\mathbf{q} = \mathbf{q}_0 e^{\lambda t} \tag{34}$$

Substituting Eq. (34) into Eq. (30), we have the global free vibration frequency equations is

$$|\mathbf{E}\lambda + \mathbf{F}| = 0 \tag{35}$$

where $\lambda = \sigma + i \cdot \omega = \sigma + i \cdot 2\pi f$ is the complex eigenvalue. ω (rad/s) is the natural whirl speeds, f (Hz) is the modal frequency of structural dynamic systems. σ represents the instability threshold when $\sigma > 0$.

4. Crack detection forward problem for short shafts

As the model-based crack detection method, there are two procedures need to be done. The first procedure is forward problem analysis, which considers the construction of a stiffness matrix exclusively for the crack section by applying linear fracture mechanics theory. Then a finite element model of the structures to compute the reasonable frequencies is necessary to make discrete relationships between natural frequencies along one direction (for example, y direction as shown in Fig. 2) and normalized crack location β and depth α. Therefore, a more precision database for crack identification is determination by surface fitting technique (in the present study, the two-dimensional least square surface fitting technique is used), as follows

$$f_j = F_j(\alpha, \beta) \quad (j = 1, 2, 3) \tag{36}$$

To analysis the forward problem, it is necessary to determine the additional crack stiffness due to the presence of the transverse crack, and insert this crack stiffness into a discrete representation of the structural system.

The localized additional flexibility can be calculated according to linear fracture mechanics theory (Gounaris and Dimarogonas, 1988). A section of a short shaft containing a crack of depth δ is shown, under general loading, in Fig. 3. P_1 is axial tension, P_2 is transverse shear, P_3 is transverse shear, P_4 is bending moment, P_5 is bending moment and P_6 is torsion. Fig. 4 shows the cross section of the cracked short shaft. The current analysis is not concerned with torsion or axial displacement, hence only c_{22}, c_{33}, c_{44}, c_{45}, c_{54}, c_{55} are required. These elements are then given by

$$c_{22} = \frac{4(1-\mu^2)}{\pi E r} \int_0^{\bar{b}} \int_0^{\bar{a}} \overline{\eta} F_{III}^2\left(\frac{\overline{\eta}}{H}\right) \mathrm{d}\overline{\eta}\,\mathrm{d}\overline{\xi} \tag{37}$$

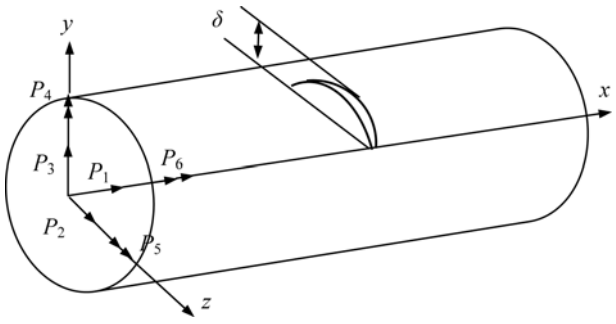

Fig. 3 Typical shaft containing a crack

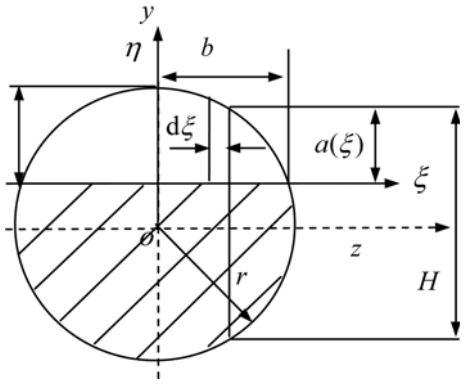

Fig. 4 Geometry of a cracked section in shaft

$$c_{33} = \frac{4(1-\mu^2)}{\pi E r}\int_0^{\bar{b}}\int_0^{\bar{a}} \bar{\eta} F_{II}^2\left(\frac{\bar{\eta}}{H}\right) \mathrm{d}\bar{\eta}\mathrm{d}\bar{\xi} \tag{38}$$

$$c_{44} = \frac{32(1-\mu^2)}{\pi E r^3}\int_0^{\bar{b}}\int_0^{\bar{a}} \bar{\xi}^2\bar{\eta} F_1^2\left(\frac{\bar{\eta}}{H}\right) \mathrm{d}\bar{\eta}\mathrm{d}\bar{\xi} \tag{39}$$

$$c_{45} = c_{54} = \frac{64(1-\mu^2)}{\pi E r^3}\int_0^{\bar{b}}\int_0^{\bar{a}} \bar{\xi}\bar{\eta}\sqrt{1-\bar{\xi}^2} F_1\left(\frac{\bar{\eta}}{H}\right) F_2\left(\frac{\bar{\eta}}{H}\right) \mathrm{d}\bar{\eta}\mathrm{d}\bar{\xi} \tag{40}$$

$$c_{55} = \frac{64(1-\mu^2)}{\pi E r^3}\int_0^{\bar{b}}\int_0^{\bar{a}} \bar{\eta}(1-\bar{\xi}^2) F_2^2\left(\frac{\bar{\eta}}{H}\right) \mathrm{d}\bar{\eta}\mathrm{d}\bar{\xi} \tag{41}$$

where $\bar{\eta}=\eta/r$, $\bar{\xi}=\xi/r$, $\bar{H}=H/r$, $\bar{a}=a/r$, $\bar{b}=b/r$, $a=2r\alpha-(r-\sqrt{r^2-\bar{\xi}^2})$, $H=2\sqrt{r^2-\bar{\xi}^2}$, $b=r\sqrt{1-(1-2\alpha)^2}$, $\alpha = \delta/2r$ denotes normalized crack depth. The corresponding intensity functions are given by (Tada *et al.* 2000)

$$\begin{cases} F_1(\eta/H) = \sqrt{\tan\lambda/\lambda}[0.752 + 2.02(\eta/H) + 0.37(1-\sin\lambda)^3]/\cos\lambda \\ F_2(\eta/H) = \sqrt{\tan\lambda/\lambda}[0.932 + 0.199(1-\sin\lambda)^4]/\cos\lambda \\ F_{II}(\eta/H) = [1.122 - 0.561(\eta/H) + 0.085(\eta/H)^2 + 0.18(\eta/H)^3]/\sqrt{1-\eta/H} \\ F_{III}(\eta/H) = \sqrt{\tan\lambda/\lambda} \\ \lambda = \pi\eta/(2H) \end{cases} \tag{42}$$

Therefore, the dimensionless flexibilities can be obtained according to

$$\begin{cases} \bar{c}_{22} = c_{22}\dfrac{\pi E r}{(1-\mu^2)},\ \bar{c}_{33} = c_{33}\dfrac{\pi E r}{(1-\mu^2)},\ \bar{c}_{44} = c_{44}\dfrac{\pi E r^3}{(1-\mu^2)} \\ \bar{c}_{45} = c_{45}\dfrac{\pi E r^3}{(1-\mu^2)},\ \bar{c}_{55} = c_{55}\dfrac{\pi E r^3}{(1-\mu^2)} \end{cases} \tag{43}$$

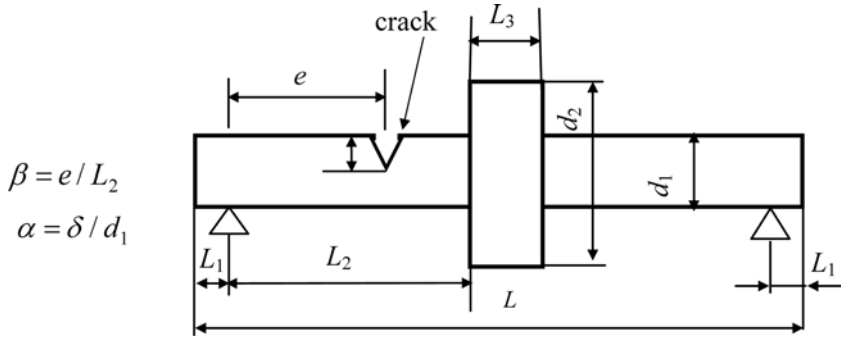

Fig. 5 Simply supported crack shaft with a rigid disc

The dimensionless compliance matrix is then

$$\bar{\mathbf{c}} = \begin{bmatrix} \bar{c}_{22} & 0 & 0 & 0 \\ 0 & \bar{c}_{33} & 0 & 0 \\ 0 & 0 & \bar{c}_{44} & \bar{c}_{45} \\ 0 & 0 & \bar{c}_{54} & \bar{c}_{55} \end{bmatrix} \tag{44}$$

Fig. 5 shows a simply supported cracked short shaft (suppose the crack occurred on segment L_2). A transverse crack of depth δ is considered on a shaft of diameter d_1 (the corresponding radius is r_1) and the normalized crack location $\beta = e/L_2$.

The inverse of the compliance matrix $\bar{\mathbf{c}}^{-1}$ is the stiffness matrix of the cracked nodal element, and the cracked stiffness submatrix $\mathbf{K}_{crack}$ can be written as (Kisa *et al.* 1998)

$$\mathbf{K}_{crack} = \begin{bmatrix} (\bar{\mathbf{c}})^{-1} & -(\bar{\mathbf{c}})^{-1} \\ -(\bar{\mathbf{c}})^{-1} & (\bar{\mathbf{c}})^{-1} \end{bmatrix}_{(8\times 8)} \tag{45}$$

The short shaft and rigid disc are modeled by BSWI rotating BSWI rotating Rayleigh-Timoshenko beam element. Hence, we can assemble cracked stiffness submatrix $\mathbf{K}_{crack}$ into the global stiffness matrix according to the corresponding DOFs easily. The global mass and gyroscope matrices of cracked short shaft are equal to the uncracked one. For the determination of the natural frequencies f for a given crack location (determine the insert location of cracked stiffness matrix $\mathbf{K}_{crack}$ in global stiffness) and depth (determine the cracked stiffness matrix $\mathbf{K}_{crack}$), the normalized crack location β and depth α are given as input. The discrete values between the natural frequencies and the crack parameters will be solved by BSWI finite element model. Then the precision crack identification database for short shaft is accomplished by least square surface-fitting techniques. Fig. 6 shows the crack identification database along y directions by using least square surface-fitting techniques for simply supported short shaft without rigid disc.

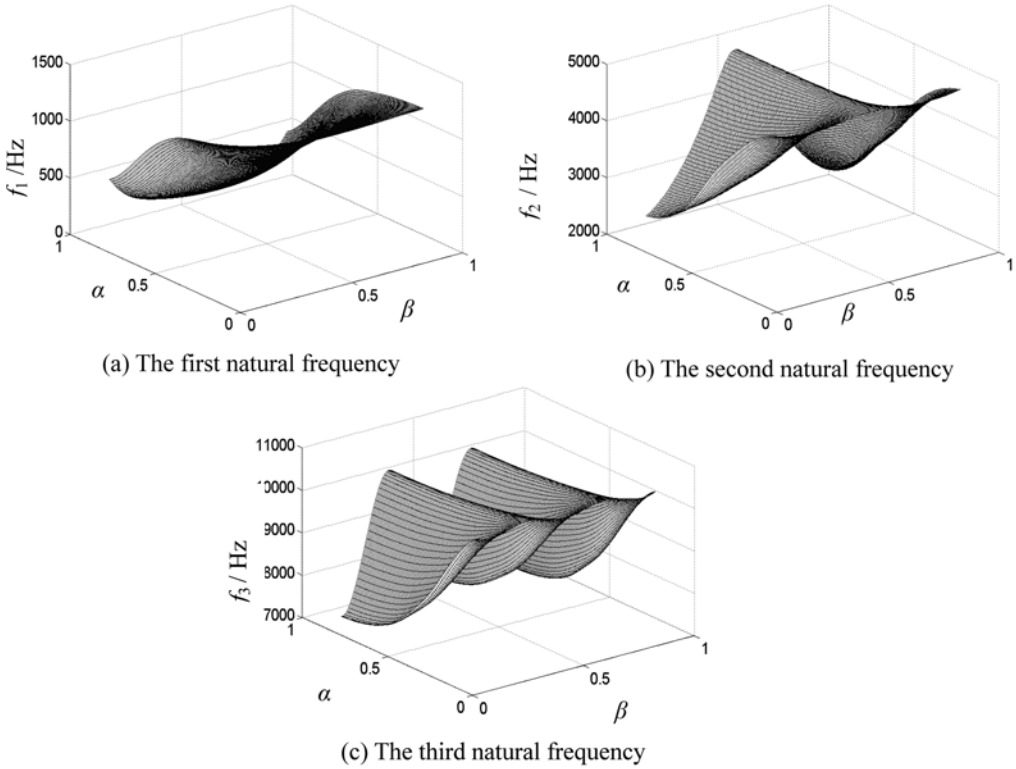

(a) The first natural frequency

(b) The second natural frequency

(c) The third natural frequency

Fig. 6 Crack identification database for simply supported short shaft without rigid disc

5. Neural networks for inverse problems

The second procedure is inverse problem analysis, which considers the measurement of dynamic parameters and numerical computing or searching for optimization values of normalized crack location and depth according to the solving results of forward problem. That is the determination the normalized crack location β and depth α, as follows

$$(\alpha, \beta) = F_j^{-1}(f_j) \qquad (j = 1, 2, 3) \tag{46}$$

The method of frequencies contour lines (Owolabi 2003, Xiang *et al.* 2006, 2007) or other methods (Lele and Maiti 2002, Murigendrappa and Maiti 2005) plus 'zero-setting' procedure (Adams *et al.* 1978) can fulfill the inverse problem of crack detection. In the 'zero-setting' procedure procedure, Young's modulus of the structure is changed by using the undamaged natural frequencies of the structure to determine an effective value. namely

$$\left| \omega_i^2 \overline{\mathbf{M}} - E_m \frac{\overline{\mathbf{K}}}{E} \right| = 0 \tag{47}$$

where E_m is the corrected value of Young's modulus E, which can be acquired through solving Eq. (47) for each frequency. This procedure can reduce the error between theoretical analysis and

the experimental studies, which are caused by boundary conditions and material parameters. However, 'zero-setting' procedure ascribes all the errors to Young's modulus, which will distort the modal parameters of a real dynamic system.

Neural networks can efficiently solve inverse problems in engineering as mentioned in introduction. Neural networks are based on models of biological neurons and form a parallel information processing array based on a networks of interconnected artificial neurons. The function of artificial neurons is similar to that of real neurons: they are able to communicate by sending signals to each other over a large number of biased or weighted connections. Each of these neurons has an associated transfer function which describes how the weighted ksum of its inputs is converted to an output. Computational models of a neural networks try to emulate the physiology of real neurons. There are two principal functions for artificial neural networks. One is the input-output mapping or feature extraction. The other is pattern association or generalization. The mapping of input and output patterns is estimated or learned by the neural networks with a representative sample of input and output patterns. The generalization of the neural networks is an output pattern in response to an input pattern, based on the networks memories that function like the human brain. Therefore, a neural networks can learn patterns from a sample data set and determine the class of new data based on previous knowledge.

Among the various types of neural networks, the multi-layer perceptron trained with the back-propagation algorithm (BP neural networks) has been proved to be most useful in engineering applications (Qu and Chen 2003, Cho and Choi 2004, Lee and Yun 2005). Thus BP neural networks is used in the present studies. The back-propagation networks is given its name due to the way that it learns by back propagating the errors in the direction from output neurons to input neurons.

The input/output relationship of the neural networks can be non-linear as well as linear, and its characteristics are determined by the synaptic weights assigned to the connections between the neurons in two adjacent layers. Fig. 7 shows the principle of crack diagnosis algorithm based on neural networks. The fist three frequencies database (i.e., the relationship between different normalized crack location and depth and the first three natural frequencies of cracked short shaft) solved by wavelet-based finite element model of cracked short shaft is employed as training samples to train the BP neural networks. Then the measured first three natural frequencies at one direction (e.g., y direction) are applied to the trained BP neural networks to quantitatively identify the real crack location and depth.

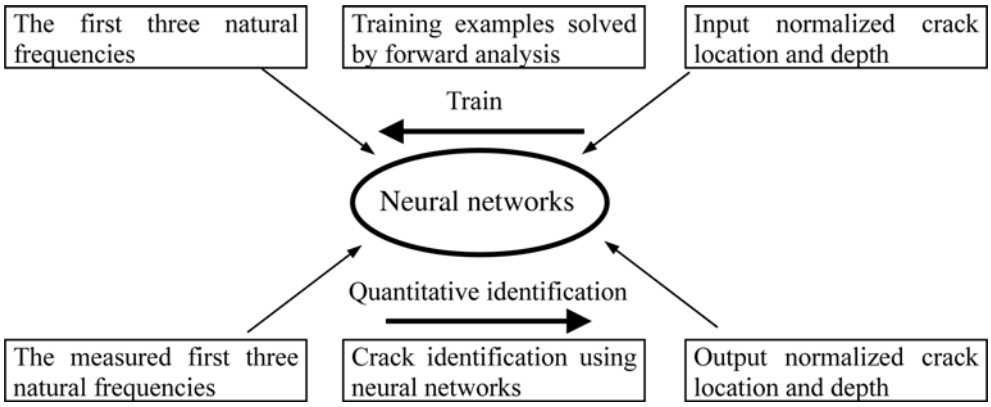

Fig. 7 Crack diagnosis algorithm based on neural networks

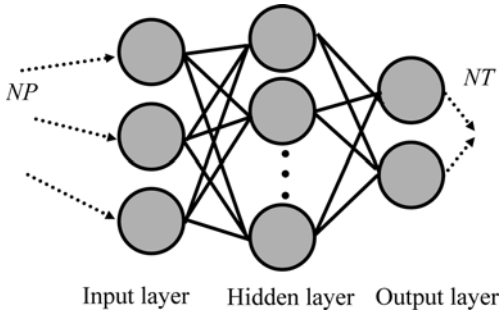

Fig. 8 The flow chart of neural networks to deal with data

Based on BP neural networks, three procedures will be done to accomplish the crack identification in short shaft, i.e., networks definition, networks train and networks identification. Fig. 8 shows the flow chart of neural networks to deal with data.

(1) Networks definition. The normalized crack location β and depth α are defined as the diagnosis parameters *NP* and the first three natural frequencies $f_r(r = 1, 2, 3)$ are served as vibration parameters *NT*. Because the high performance of BSWI element, we can get a high precision cracked identification database by forward problem analysis. Therefore, the little input nodes and small networks scale are needed to train a stability and robust BP neural networks.

(2) Networks train. A pair of *NP* and f_r is employed as training samples to train neural networks for crack identification in short shafts. The first three natural frequencies $f_r(r = 1, 2, 3)$ of short shaft computed by wavelet-based model are served as inputs parameters while the normalized crack location β and depth α are looked as outputs parameters. Then compute specific mean-square training errors with standard procedures and iterations constantly. And terminating the training process when output parameters equal to target parameters or the errors between output parameters and target parameters satisfy the threshold values.

(3) Networks identification. The measured first three frequencies of real cracked short shaft are applied to the trained BP neural networks to gain the normalized crack location β and depth α though networks computing.

6. Experimental studies

Fig. 9 shows the experimental setup used for measuring the first three frequencies of the cracked shaft with a single mass disc using the Doppler signal laser vibrometer. A Polytec Doppler laser vibrometer OFV-505/5000 is used to measure the velocities of one point in the shaft and a hammer is used to excite the rotor systems at the other point. In order to gain a reality measured frequencies, 100 data sets are recorded to solve an average frequencies values.

Some sawed short shafts with width 0.02 mm are used. The six crack cases are shown in Table 1. The material of workpiece for experiment is 40Cr steel, and the simply supported short shaft geometries and material properties are: $L = 154$ mm, $L_1 = 8$ mm, $L_2 = 60$ mm, $L_3 = 18$ mm, $d_1 = 30$ mm, $d_2 = 100$ mm, Young's modulus $E = 2.06\times10^{11}$ N/m^2, material density $\rho = 7860$ kg/m^3, Poisson's ratio $\mu = 0.3$, the shear modulus $G = 80$ GPa, the shear deformation coefficient $k = 10/9$.

Fig. 10 shows the crack identification database for the experimental short shaft systems. That is

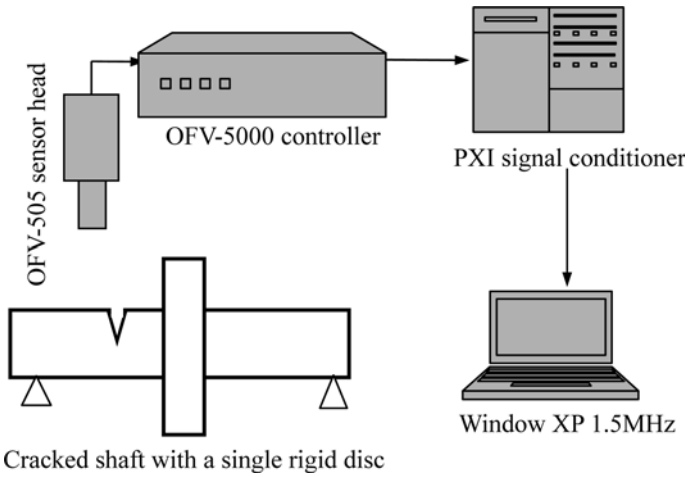

Fig. 9 Testing principle diagram

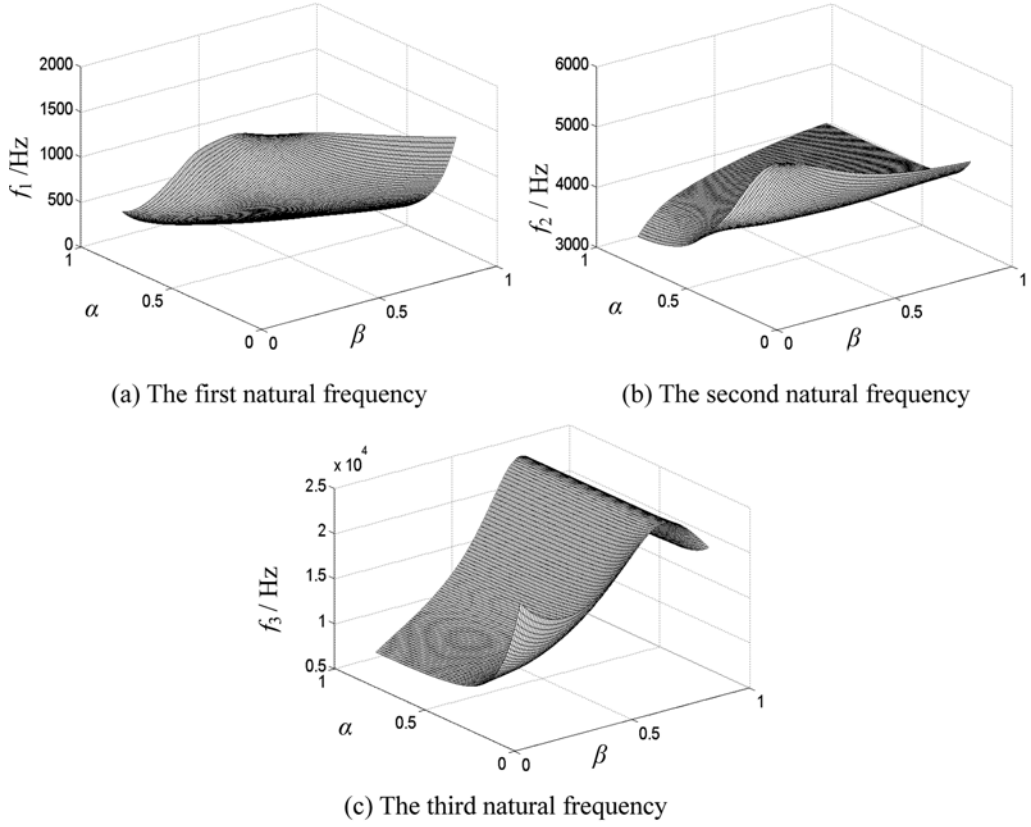

Fig. 10 Crack identification database for the experimental short shaft systems

the relationship between $f_i(i = 1, 2, 3)$ and all possible normalized crack location β and depth α by using wavelet-based finite element model and the least square surface fitting techniques (Here,

Table 1 Crack cases of short shaft and identification results

Case	β	α	Measured frequencies/Hz			Predicted β* (Error/%)	Predicted α* (Error%)
			f_1/Hz	f_2/Hz	f_3/Hz		
1	0.4	0.2	1331.1	4384.9	14160.1	0.42(5)	0.18 (10)
2	0.4	0.4	715.3	4011.7	13040.1	0.38 (5)	0.42 (5)
3	0.6	0.2	1048.5	4329.4	15129.6	0.58 (3.3)	0.23 (15)
4	0.6	0.4	698.3	4139.3	15653.3	0.63 (5)	0.38 (5)
5	0.5	0.2	1176.4	4330.8	14529.1	0.83 (3.8)	0.22 (10)
6	0.5	0.4	679.2	4088.7	15517.3	0.79 (1.3)	0.42 (5)

Notes: Error/% is calculated by $|\beta^*-\beta|/\beta\times 100\%$ or $|\alpha^*-\alpha|/\alpha\times 100\%$

$\alpha, \beta = [0.05, 0.9]$). The standard procedures of BP neural networks for inverse problems analysis are applied to solve the inverse problem of experimental shafts.

Table 1 shows the comparison of actual normalized crack parameters β and α and the predicted crack parameters β^* and α^*. For the given cases, the relative errors of β^* are not more than 5% while the relative errors of α^* arrive at 10%. Hence, the proposed model-based crack identification method by using wavelet-based element and neural networks is considered to be valid for applying to detect cracks in short shafts. Because the good characteristics of BSWI scaling functions, such as multi-resolution analysis and localization, the presented element have higher efficiency and precision to deal with high performance computing in engineering. Therefore, fewer wavelet-based elements are needed to construct higher finite element model of structural dynamic systems. And the model-based inverse problems are solved by BP neural work, which is a robust and stability way to deal with inverse problem for crack detection in short shafts. In addition, the BSWI rotating Rayleigh-Timoshenko element can also employed as a useful tool to solve rotor dynamics not only for short shaft but also for slender shaft. The reason is that C_0 type BSWI element has the ability to resist shear-locking phenomenon (Xiang *et al.* 2007).

7. Conclusions

The strategies and procedures of crack identification of short shaft are proposed by combining BSWI rotating Rayleigh-Timoshenko beam element and BP neural networks. The present studies developed a new wavelet-based beam element for analysis short shafts. By applying linear fracture mechanics theory, the wavelet-based finite element model of short shafts can be built up to gain more accurate natural frequencies of the cracked structural systems. A precise crack identification database is also obtained by using the least square surface fitting technique. For solving the inverse problem, the BP neural networks is employed as an efficient tool to gain a robust and stability crack identification results. The experimental results of cracked short shaft have demonstrated that the present method is a useful and robust way to identify the crack location and size in short shaft.

It remain some problems should be considered in the future. Firstly, the key to successful applying the present method to on-line monitor and diagnosis cracks in short shaft is the operational modal analysis (OMA) techniques to extract the exact modal parameters. Therefore, bearing stiffness and damp will be considered in the future work. Secondly, for the detection of multiple

cracks, the different crack orientations should be considered to make a more reasonable results.

Acknowledgements

Authors are gratefully acknowledging the financial support by the project of National Science Foundation of China (Nos. 50805028, 50875195), Open Foundation of the State Key Laboratory of Structural Analysis for Industrial Equipment (No. GZ0815), Youth Science Foundation of GuangXi Province (No.0832082), GuangXi Key Laboratory of Manufacturing System & Advance Manufacturing Technology (No. 0842006_023_ Z).

References

Adams, R.D., Cawley, P., Pye, C.J. and Stone, B.J. (1978), "A vibration technique for non-destructively assessing the integrity of structures", *J. Mech. Eng. Sci.*, **20**(2), 93-100.

Canuto, C., Tabacco, A. and Urban, K. (1999), "The wavelet element method part I: Construction and analysis", *Appl. Comput. Harmon. A.*, **6**, 1-52.

Canuto, C., Tabacco, A. and Urban, K. (2000), "The wavelet element method part II: Realization and additional feature in 2D and 3D", *Appl. Comput. Harmon. A.*, **8**, 123-165.

Cho, H.N., Choi, Y.M., Lee, S.C. and Hur C.K. (2004), "Damage assessment of cable stayed bridge using probabilistic neural networks", *Struct. Eng. Mech.*, **17**(3-4), 483-492.

Chui, C.K. and Quak, E. (1992), "Wavelets on a bounded interval", *Numer. Method. Approx. Theory*, **1**, 53-57.

Dimarogonas, A.D. (1996), "Vibration of cracked structures: a state of the art review", *Eng. Fract. Mech.*, **55**(5), 831-857.

Doebling, S.W., Farrar, C.R. and Prime, M.B. (1998), "A summary review of vibration-based damage identification", *Shock Vib.*, **30**(2), 91-105.

Goswami, J.C., Chan, A.K. and Chui, C.K. (1995), "On solving first-kind integral equations using wavelets on a bounded interval", *IEEE T. Antenn. Propag.*, **43**, 614-622.

Gounaris, G. and Dimarogonas, A.D. (1988), "A finite element of a cracked prismatic beam for structural analysis", *Comput. Struct.*, **28**, 309-313.

Green, I. and Casey, C. (2005), "Crack detection in a rotor dynamic system by vibration monitoring-Part I: Analysis", *J. Eng. Gas Trub. Power*, ASME, **127**, 425-436.

Han, J.G., Ren, W.X. and Huang, Y. (2006), "A spline wavelet finite element method in structural mechanics", *Int. J. Numer. Meth. Eng.*, **66**, 166-190.

Kisa, M., Brandon, J. and Topcu, M. (1998), "Free vibration analysis of cracked beams by a combination of finite elements and component mode synthesis methods", *Comput. Struct.*, **67**, 215-223.

Lee, J.J., Lee, J.W., Yi, J.H., Yun, C.B. and Jung, H.Y. (2005), "Neural networks-based damage detection for bridges considering errors in baseline finite element models", *J. Sound Vib.*, **280**, 555-578.

Lee, Y.S. and Chung, M.T. (2000), "A study on crack detection using eignfrequency test data", *Comput. Struct.*, **77**, 327-342.

Lele, S.P. and Maiti, S.K. (2002), "Modeling of transverse vibration of short beams for crack detection and measurement of crack extension", *J. Sound Vib.*, **257**(3), 559-583.

Liu, S.W., Huang, J.H., Sung, J.C. and Lee, C.C. (2002), "Detection of cracks using neural networks and computational mechanics", *Comput. Meth. Appl. Mech. Eng.*, **191**, 2831-2845.

Montalvão, D., Maia, N.M.M. and Ribeiro, A.M.R. (2006), "A review of vibration-based structural health monitoring with special emphasis on composite materials", *Shock Vib.*, **38**(4), 1-30.

Murigendrappa, S.M., Maiti, S.K. and Srirangarajian, M.R. (2005), "Detection of crack in L-shaped pipes filled with fluid based on transverse natural frequencies", *Struct. Eng. Mech.*, **21**(6), 635-658.

Nandwana, B.P. and Maiti, S.K. (1997), "Detection of the location and size of a crack in stepped cantilever

beams based on measurements of natural frequencies". *J. Sound Vib.* , **203**(3), 435-446.
Nelson, H.D. (1980), "The dynamics of rotor-bearing systems using finite element", *J. Mech. Des.*, ASME, **102**, 793-803.
Owolabi, G.M., Swamidas, A.S.J. and Seshadri, R. (2003), "Crack detection in beams using changes in frequencies and amplitudes of frequency response functions", *J. Sound Vib.*, **265**, 1-22.
Papadopoulos, C.A. and Dimarogonas, A.D. (1987), "Coupled longitudinal and bending vibrations of a rotating shaft with an open crack", *J. Sound Vib.*, **117**(1), 81-93.
Qu, W.L., Chen, W. and Xiao, Y.Q. (2003), "A two-step approach for joint damage diagnosis of framed structures using artificial neural networks", *Struct. Eng. Mech.*, **16**(5), 581-595.
Sekhar, A.S. and Srinivas, B.N. (2002), "Vibration characteristics of slotted shafts", *J. Sound Vib.*, **251**(4), 621-630.
Sinou, J.J. (2007), "A robust identification of single crack location and size only based on pulsations of the cracked system", *Struct. Eng. Mech.*, **25**(6), 691-716.
Tada, H., Paris, P.C. and Irwin, G.R. (2000), *The Stress Analysis of Cracks Handbook* (3rd edition). New York, ASME Press.
Xiang, J.W., Chen, X.F., He, Y.M. and He, Z.J. (2006a), "The construction of plane elastomechanics and Mindlin plate elements of B-spline wavelet on the interval", *Finite Elem. Anal. Des.*, **42**, 1269-1280.
Xiang, J.W., Chen, X.F., He, Y.M. and He, Z.J. (2007a), "Static and vibration analysis of thin plates by using finite element method of B-spline wavelet on the interval", *Struct. Eng. Mech.*, **25**(5), 613-629.
Xiang, J.W., Chen, X.F., He, Z.J. and Dong, H.B. (2007b), "The construction of 1D wavelet finite elements for structural analysis", *Comput. Mech.*, **40**(2), 325-339.
Xiang, J.W., Chen, X.F., He, Z.J. and Zhang, Y.H. (2007c), "A new wavelet-based thin plate element using B-spline wavelet on the interval", *Comput. Mech.*, **41**(2), 243-255.
Xiang, J.W., Chen, X.F., Li, B., He, Y.M. and He, Z.J. (2006), "Identification of crack in a beam based on finite element method of B-spline wavelet on the interval", *J. Sound Vib.*, **296**(4-5), 1046-1052.
Xiang, J.W., Chen, X.F., Mo, Q.Y. and He, Z.J. (2007), "Identification of crack in a rotor system based on wavelet finite element method", *Finite Elem. Anal. Des.*, **43**(14), 1068-1081.
Yuan, S.F., Wang, L. and Peng, G. (2005), "Neural networks method based on a new damage signature for structural health monitoring", *Thin Wall. Struct.*, **43**, 553-563.
Zachiarias, J., Hartmann, C. and Delgado, A. (2004), "Damage detection on crates of beverages by artificial neural networks trained with finite-element data", *Comput. Meth. Appl. Mech. Eng.*, **193**, 561-574.